Application of support vector machine for prediction of electrical and thermal performance in PV/T system

Juwel Chandra Mojumder [a], Hwai Chyuan Ong [a,*], Wen Tong Chong [a], Shahaboddin Shamshirband [b,*], Abdullah-Al-Mamoon [a]

[a] Department of Mechanical Engineering, Faculty of Engineering, University of Malaya, Kuala Lumpur 50603, Malaysia
[b] Department of Computer Systems and Information Technology, Faculty of Computer Science and Information Technology, University of Malaya, Kuala Lumpur 50603, Malaysia

ABSTRACT

In photovoltaic–thermal (PV/T) system analysis, solar collectors with numerous design concepts have been used to purvey the thermal and electrical energy effectively. In this study, two types of solar thermal collectors in PV/T system are proposed and fabricated called design A and design B respectively. In order to investigate the effects of collector type on the system performance a thin flat metallic sheet (TFMS) and fins were introduced as an effective heat absorber and heat sink in the collectors. Extensive experiments were carried out for different conditions under indoor solar simulator. Then PV/T thermal and electrical efficiency were calculated by using data obtained from experiments. Here, support vector machine (SVM) model is designed to estimate the thermal and electrical output which predicts the values for some input variables. For this purpose, three SVM models namely SVM coupled with the discrete wavelet transform (SVM-Wavelet), the firefly algorithm (SVM-FFA) and with using the radial basis function (SVM-RBF) were analyzed. The estimation and prediction results of these models were compared with each other using statistical indicators i.e. root means square error, coefficient of determination and Pearson coefficient. The experimental results show that a significant improvement in predictive accuracy and capability of generalization can be achieved by the SVM-Wavelet approach. Moreover, the results indicate that proposed SVM-Wavelet model can adequately predict the electrical and thermal efficiencies of PV/T system. In the final analysis, a proper sensitivity analysis is performed to identify the influence of considered input elements on performance prediction of PV/T system.

© 2015 Elsevier B.V. All rights reserved.

1. Introduction

Solar energy is considered as the most reliable energy source in nature for harvesting in different areas, which can reduce our dependence on fossil fuels and also helps in reducing greenhouse gas emissions. The application of solar energy is mainly classified in two categories by solar thermal and photovoltaic system [1]. Then, it is also included the combined solar photovoltaic-thermal energy (PV/T) in order to utilize the wasted heat energy [2]. Solar air collector (SAC) is considered as the key component of harnessing thermal energy from any solar energy systems, described by Caner et al. [3]. PV/T is gaining popularity in building technology due to simultaneous electrical and thermal output from the same system.

For example, the thermal energy output has been used in heating domestic hot water [4], building thermal heating [5], heat pump [6] etc. Meanwhile, the building-integrated photovoltaic with thermal energy recovery system (BIPV/T) is growing fast day by day to harness solar energy to meet the optimal integration of renewable energy [7]. PV/T has been shown as main part of the BIPV/T design [8], where the photovoltaic (PV) cell can convert solar radiation to electricity and the rest is converted to heat [9]. Researchers have introduced different PV/T design concept to achieve optimum electrical and thermal output. The outputs are mostly dependent on the photovoltaic internal-external factors and the types of thermal collectors respectively [10].

PV efficiency falls when PV cell temperatures increases which is pointed by Vera et al. [11]. In order to develop the solar PV efficiency, water and air have been used concurrently for cooling systems. A wide research met satisfactory result by using several fluids as a heat transport medium in collectors, but mostly focused on water [12–14], air [15–17] type PV/T collectors, also refrigerant (R410a) was used as the working fluid by Shan et al. [18]. Hybrid

* Corresponding authors. Tel.: +60 16 590 3110/3 7967 5247; fax: +60 3 7967 5317..
  E-mail addresses: onghc@um.edu.my (H.C. Ong), shamshirband1396@gmail.com (S. Shamshirband).

Nomenclature

ANN   artificial neural networks
BIPV/T   building integrated photovoltaic thermal
PV/T   photovoltaic thermal
PV   photovoltaic
RBF   radial basis function
RMSE   root means square error
SAC   solar air collector
SVM   support vector machine
TFMS   thin flat metallic sheet
$A_{c.t}$ collector area (m^2)
b scalar
C_a specific heat (J/kg/K)
G irradiation (W/m^2)
$\dot{m}_a$ mass flow rate (kg/m^3)
Q_u useful heat transfer rate (W)
R_2 coefficient of determination
r Pearson coefficient
T_{in} collector inlet temperature (°C)
T_{out} collector outlet temperature (°C)
T_f collector mean air temperature (°C)
v air flow velocity (m/s)
x input space vector

Greeks
$\varphi(X)$ high dimensional space
Υ, ε and C RBF parameters
ξ_i positive slack variables
η efficiency
ρ fluid density (kg/m^3)

Subscript
a air
c pv cell
f fluid
in   inlet
th   thermal
o overall
out   outlet
ref   reference

heat absorber fluid (water and air) was used in PV/T system which was strongly established by Zondag et al. [19]. In terms of easy operation and maintenance, air is considered as more suitable than water type cooling fluid and power consumption is less compared with water cooling, concluded by Tonui et al. [20]. In some rigorous reviews, recent development and applications of PV/T were discussed on the various configurations with several augmented methods of flat plate PV/T collector models [2,21–24]. In addition, some effective ways can be used to increase the convective heat transfer effect inside the collector channel, such as using corrugated polycarbonate material [25], graphite material [26], galvanized steel [17] and phase change materials (PCM) [27].

Again, the support vector machine (SVM), one of the novel soft computing learning algorithms, has found wide applications in different fields [28–31]. Furthermore, it has been majorly applied in pattern recognition, forecasting, classification and regression analysis [32–34]. The most commonly used kernels include linear, polynomial inner product functions and the radial basis function (RBF). The selection of a kernel function largely depends on the nature of the observed data [35]. Biological inspired metaheuristic optimization algorithms such as ant colony optimization (ACO), genetic algorithm (GA), particle swarm optimization (PSO) and

cuckoo search (CS) have found wide applications in different field of science [36–40]. These algorithms are based on the mechanism of selection of the fittest in biological systems. A more recent approach in biological inspired metaheuristic optimization algorithms is firefly algorithm (FFA) developed by Yang [41]. The FFA has been adjudging to be more efficient and robust in finding both local and global optima compare to other biological inspired optimization algorithms [42–45]. The prediction accuracy of the SVM model highly relies on proper determination of model parameters. Although organized strategies for selecting parameters are important, model parameter alignment also need to be made. In this study, the FFA is used for determination of SVM parameters.

The numbers of experimental investigations on flat plate PV/T collectors have been carried out since the late 1970s and more importantly, ANN technique was used in prediction of the flat plate solar collector performance [46]. The use of artificial intelligence methods in many application of thermal system performance analysis increases gradually such as in calculating the thermal performance of SAC. Artificial neural network (ANN) method gives some satisfactory predicted results proposed by Caner et al. [3], the method was working based on the data classification by training, validation and testing under eight inputs and single output variable. Again, a series of prediction model was developed by Varol et al. [27]. But SVM showed more popularity which is widely used machine-learning tools comparing with neural networks claimed by Esen et al. [47]. They recommended using SVM as a good, intelligent method in the case study of ground coupled heat pump (GCHP) for space heating purposes. In addition to the parametric analysis, SVM was modeled using five inputs and one output. The result shows that the SVM could predict co-efficient of performance (COP) effectively. The authors also intended to adopt the analysis in finding the system efficiency for modeling using least-square support vector machine (LS-SVM) [48], artificial neural network (ANN) and wavelet neural network (WNN) models [49] for three types of solar air heater (SAH).

In this study, the SVM was coupled with discrete wavelet transform. Wavelet transform (WT) has many useful basis functions to select from depending on the signal that is being analysed. Wavelet analysis was used to decompose the time series of data into its various components, after which the decomposed components can be used as inputs for the SVM model. Over the past few years, this technique has become of enormous interest in engineering applications [50,51].

The conventional algorithms employed for calculating thermal efficiency are usually complicated in solving the mathematical form because it involves the complex in solution for differential equations developed from thermal balance relation and individual part analysis in PV/T system [13,15,16,19,52–54]. All the energy calculation is based on the thermal interaction of heat flow between a flowing fluid and the collector body under steady state flow condition because the thermal performance depends on collector material, space, dimension and layout [3]. As a result, it appears some statistical error in proper curve fitting between theoretical and experimental values for various measurement, heat loss and uncertainty in the collector as well. In this case, SVM is used to overcome the complex mathematical form and mathematical routines found in classical methods of PV/T. It helps to learn the original information patterns within a multi-dimensional information domain and helps to eliminate long series of collector performance test.

Soft computing technology has been applied effectively in many different fields of engineering application due to their attractive capabilities in forecasting, modeling of complex nonlinear systems and achieving the optimum efficiencies. As mentioned, the PV/T technology has some remarkable benefits and several PV/T collector designs have been proposed and developed within the
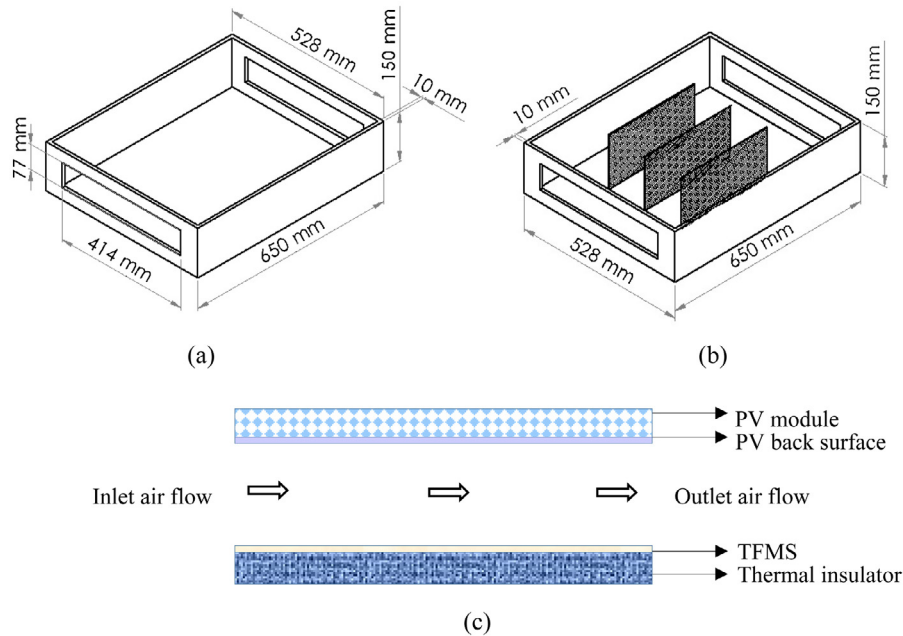
Fig. 1. PV/T collectors (a) design A, with TFMS (b) design B, used fins and TFMS (c) collector air flow diagram.

last few decades ago. However, it is not a mature technology yet. It is still requires further study for estimating the thermal and electrical efficiency using less number of input variables for future BIPV/T design improvement, faster payback than traditional systems. Thus, motivating by such needs and realizing the rising popularity of the SVM regression application and good predictions can be obtained from the SVM-Wavelet model as a new platform in applied PV/T research. This paper presents a study to construct, develop and evaluate the results of SVM-Wavelet, SVM-FFA and SVM-RBF for electrical and thermal efficiency of two air type's flat plate PV/T system with more effectively.

2. Methodology

2.1. Performance parameters analysis

In the present study of the PV/T system, proposed two types of collector which is shown in Fig. 1(a) and (b) and the collector flow diagram in Fig. 1(c). In many cases, experimental value is compared with the theoretical value for different types of the PV/T collector design. This is a more conventional way to draw the relation between the actual and predicted value of thermal and electrical efficiency. Thermal balance equations for all the layers in the PV/T collector carried out the thermal characteristics in PV/T collectors. The details of governing equation for PV/T which theoretically insists to get the temperature from different layers of PV/T such as photovoltaic cell, rear PV surface, back wall surface, collector inlet and outlet. Besides this, some assumption should be considered for energy balance equations although having some limitations in practical cases. Such as (1) a mean temperature is assumed across each layer (2) back wall surface (Design A and B), fin surface (Design B) temperatures were taken as a uniform on the entire working area (3) heat capacities of PV back surface, solar cell material, collector and insulation materials was neglected (4) one dimensional heat conduction and the system is in quasi-steady state. Beyond this, dynamic analysis shows the fairly complex relation to the definition of various thermal relations and some other constructional parameters are related to collecting useful energy from SAC.

2.2. Performance analysis

Solar irradiation is considered as the prime heat source in the collector which is incident on the PV panel surface. The portion of incoming irradiance is absorbed by the PV/T layers and the rest is transferred to the working fluid. The thermal efficiency (η_{th}) is mostly relied on the useful collected heat (Q_u) and the leaving air temperature (T_{out}) under the certain mass flow rate in collector channel. This thermal efficiency (η_{th}) is generally considered as the instantaneous efficiency in the PV/T system due to instantaneous operating conditions such as solar irradiance, ambient temperature, the wind speed etc.

The basic parameter can be defined as the ratio of the useful energy delivered to the energy incident on the collector aperture [55]. The relation can be shown as:

$$\eta_{th} = \frac{Q_u}{A_{c.t}G} \tag{1}$$

And,

$$Q_u = \dot{m}_a C_a (T_{out} - T_{in}) \tag{2}$$

It was assumed that the air temperature in the channel varies linearly in the flow direction so that the mean air temperature (T_f) required fixing the air properties in the channel. Then the mean air temperature (T_f) can be written as follows:

$$T_f = \frac{T_{in} + T_{out}}{2} \tag{3}$$

In the system, collector area ($A_{c.t}$), and air specific heat (C_a) is considered as constant, then the relation between thermal efficiency and other parameters can be defined as follows [56].

$$\eta_{th} = f(T_{out}, T_{in}, G, \dot{m}) \tag{4}$$

Fluid density is dependent parameter which is related to pressure and fluid temperature. In addition, mass flow rate act as a function of air velocity, which can be calculated using the following equation:

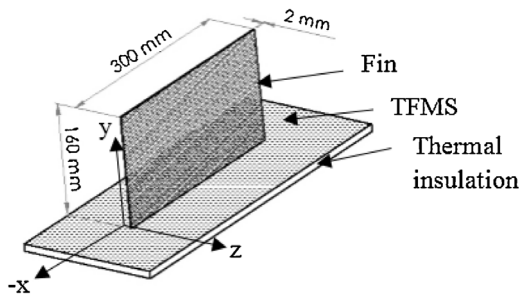$$\dot{m}_f = \rho_f A_{c.t} v \tag{5}$$

Fig. 2. Schematic diagram showing fin dimensions.

The use of fins at the collector back wall shows more practical in design and gives superior result as a heat sink medium. The thermal relation was described mathematically for number of fins used in the collector by Tonui et al. [57].

The overall fin effectiveness depends on the number of fins per unit length (fin density) as well as the individual fin effectiveness. Fig. 2 illustrates 3-dimensional diagram of a single rectangular fin representing the fin arrays that were integrated with TFMS (thermal conductivity 385 W/m/K) used in the proposed designs with individual dimensions. An aluminium bubble foil was primarily selected as an insulation material. Insulation was applied at the inner surface of thin flat metallic sheet to avoid any kind of heat transfer and losses from the collector setup. Because all kind of losses from the system decreases the overall efficiency of the PV/T system.

Some assessment was developed to calculate the PV electrical efficiency. Many studies claim that the temperature of the PV module strongly affects its energy performance as it is the function of adverse relationship between PV cell temperature and electrical efficiency. To define panel photovoltaic performance in PV/T

analysis, linear correlation is developed, the efficiency of the PV cell at T_c is given by the following [5,14,20,58].

$$\eta_{pv} = \eta_{c,ref} \left[1 - \beta_{ref}(T_c - 25\,°C) \right] \tag{6}$$

where $\eta_{c,ref}$ is the cell reference efficiency at reference temperature (25 °C), β_{ref} is the temperature coefficient which is equivalent to $0.0045\,°C^{-1}$ [55].

The electrical energy (kW h) generated from PV module is not equal with the heat energy (kW h) obtained from the collector, due to two different forms of energy. Here, the authors directly convert the conventional electrical efficiency to thermal efficiency equivalent through the following relation:

$$\eta_{th,electrical} = \frac{\eta_{PV}}{\eta_{e,power}} \tag{7}$$

where electric power generation factor ($\eta_{e,power}$) was taken as 0.38, suggested by Huang et al. [59]. So, the quantity of overall thermal efficiency (η_o) for PV/T SAC can be expressed as the sum of thermal efficiency (η_{th}) and the thermal efficiency equivalent of electrical efficiency ($\eta_{th,electrical}$) [54].

$$\eta_o = \eta_{th,electrical} + \eta_{th} \tag{8}$$

2.3. Experimental setup and system description

For experimental setup in an indoor solar simulator, a single 40 W photovoltaic panel (0.62 m × 0.50 m) was chosen. During this investigation, the solar cell type of module is poly crystalline Si that works in the temperature range between −40 °C to 85 °C. Two lead acid batteries (12 V, 24 Ah) are connected in parallel, which are the primary storage in the PV/T system (Fig. 3). Fan control unit consists with variable resistance (VR), induces different mass flow rate run by DC output connected with a solar controller (CMP24, 12V-20A). Inverters and other AC appliances were not connected in the experimental investigation.
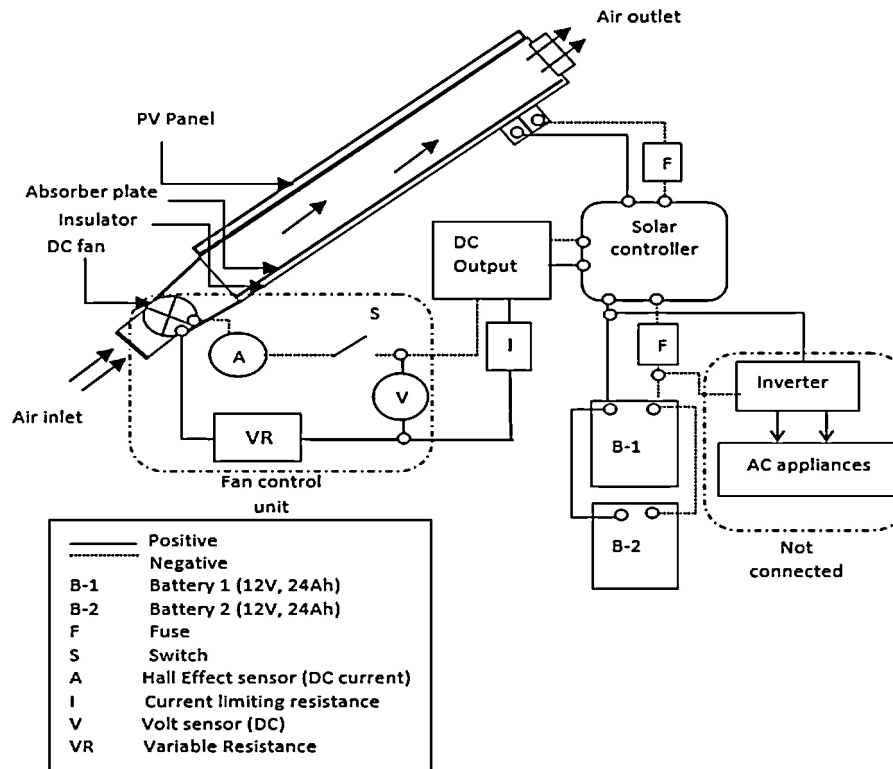

Fig. 3. Complete PV/T connection diagram.

Table 1
Some technical features for PV/T collector design.

	Values
PV module parameters	
PV module area	0.31 m²
Solar cell area	0.0069 m²
Maximum voltage (V_{max})	17.4 V
Maximum current (I_{max})	2.30 A
Fill factor (FF)	0.73
Open circuit voltage (V_{oc})	21.5 V
Short circuit current (I_{sc})	2.53 A
Operating temperature	−40 °C to 85 °C
Collector parameters	
Length	0.63 m
Width	0.51 m
Height	0.13 m
Tilt angle	25°
Cross sectional area	0.065 m²
Fin geometry parameters	
Length	0.3 m
Height	0.16 m
Thickness	2×10^{-3} m
Thermal conductivity	205 W/m/K
Fin inter spacing	0.125 m
Others	
DC fan	24 V and 0.12 A in DC

1. Initially, 18 numbers of K-type thermocouple sensors with ±0.2 °C calibrated accuracy was used to measure the temperatures of PV cell and rear surfaces, collector inlet and outlet, collector back wall surfaces. All the temperatures were read out and saved in 4-channel temperature meter data logger.
2. Electrical DC fan provides the required mass flow to the channel for both designs in terms of force circulation process. Conventional instrument know as hot wire thermo-anemometer (Extech product, working range: 0.2–50 m/s) measures the collector outlet air velocity.
3. Incoming solar radiation from halogen bulb is measured using pyranometer (data logging device, TES,1333R).

Some other useful parameters such as maximum voltage and current, open circuit voltage and current values were shown in Table 1, while the test was performed under standard test condition i.e. solar radiation value is 1000 W/m², ambient temperature is 25 °C.

2.4. Input and output variables

The effect of mass flow rate comprises the relative changes in useful heat gain. In order to produce more useful thermal power, higher flow rate gives a significant result. Because, outlet air temperature is decreased when the air velocity increases, due to taking the less contiguity time between collector heat transfer walls and the working fluid during flow. Electrical efficiency noticeably drops with the rise in PV module cell temperature. Table 2 shows the temperature distribution in different parts of solar thermal collector for design A ($G = 700$ W/m², January 28, 2015) and design B ($G = 700$ W/m², January 28, 2015) under four active mass flow rates $\dot{m}_1$ (0.04 kg/s), $\dot{m}_2$ (0.12 kg/s), $\dot{m}_3$ (0.20 kg/s), $\dot{m}_4$ (0.28 kg/s).

The temperature for all input parameters provided increases with time. As can be seen from the literature data, theoretically estimated PV cell temperature is useful to get the electrical efficiency, using Eq. (6) and collector inlet-outlet temperature difference is for thermal efficiency calculation using Eq. (1) as mentioned earlier. The average surface temperature on fins was calculated using the existing relationship for force convection and radiation, which makes higher heat transfer for design B. Table 2 illustrates the input–output variables in terms of the definition for estimating the electrical and thermal efficiency in PV/T system for both designs. In collector design, 20 sets of temperature data was obtained from experimental work for different input parameters. But parameter characterization was defined by maximum and minimum values for useful input parameters such as the mass flow rate ($\dot{m}$), inlet temperature (T_{in}), and outlet temperature (T_{out}) to calculate the overall thermal efficiency (η_o) as an output parameter. Similarly, the mass flow rate ($\dot{m}$) and PV cell temperature (T_c) are input parameters for calculating electrical efficiency (η_{PV}). All data's shown in Table 2 is based on the experimental data provided in Figs. 4 and 5, which have been employed to train the SVM prediction models by MATLAB software package. The SVM approximates the data and therefore it can be relied on in predicting the performance calculation.

2.5. Soft computing methodologies

2.5.1. Support vector machine

Support Vector Machine (SVM) [60] is based on the principle of statistical machine learning process and structural risk minimization. It minimizes the upper bound generalization error rather than local training error. This is one of the advantages of SVM over the traditional machine learning methodologies. Other advantages include unique solution due to the convex nature of the optimal problem, the use of high dimensional spaced set of kernel functions which discretely comprises non-linear transformation. Hence, no assumption in functional transformation which makes data linearly separable indispensable.

Assuming a set of data points is given by $\left\{ x_i, d_i \right\}_i^n$, where x_i is the input space vector of the data sample, d_i is the target value and n is the data size. SVM approximates the function as follows:

$$f(x) = w\varphi(x) + b \tag{9}$$

$$R_{SVMs}(C) = \frac{1}{2}||w^2|| + C\frac{1}{n}\sum_{i=1}^{n}L(x_i, d_i) \tag{10}$$

where $\varphi(x)$ is a high dimensional space feature that mapped the input space vector x, w is a normal vector, b is a scalar and $C\left(1/n\right)\sum_{i=1}^{n}L(x_i, d_i)$ erepresents the empirical error. The parameters w and b can be estimated by minimization of regularized risk function after introduction of positive slack variables ξ_i and ξ_i^* which represent upper and lower excess deviation, respectively.

$$\text{Minimize } R_{SVMs}\left(w, \xi^*\right) = \frac{1}{2}||w||^2 + C\sum_{i=1}^{n}(\xi_i + \xi_i^*) \tag{11}$$

Table 2
Input parameters for experimental power prediction.

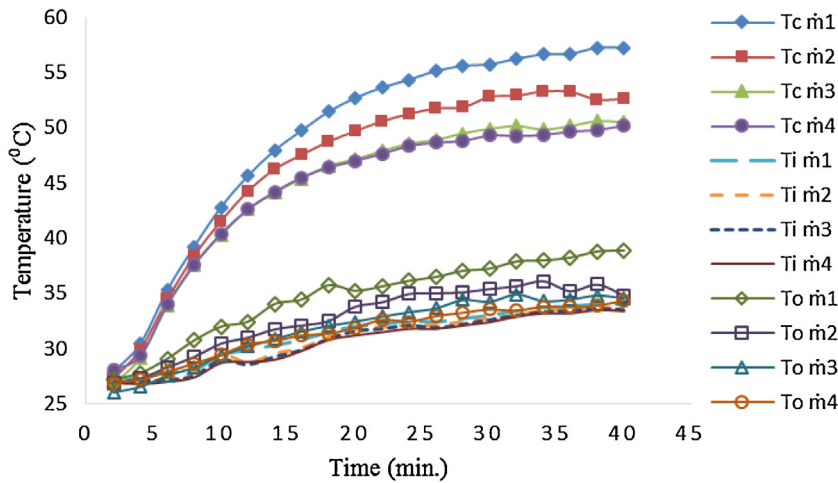| Inputs	Parameters description	Parameters characterization							
		Design A (max.–min.)				Design B (max.–min.)			
1	Mass flow rate (kg/s)	0.04	0.12	0.20	0.28	0.04	0.12	0.20	0.28
2	Inlet temperature (°C)	34.00–27.20	33.60–27.10	33.50–27.00	33.40–26.90	34.00–27.20	33.60–27.10	33.50–27.00	33.40–26.90
3	Outlet temperature (°C)	38.90–27.25	34.80–26.90	34.55–26.05	34.35–26.90	44.80–26.15	44.80–28.50	44.30–26.30	42.60–24.20
4	PV cell temperature (°C)	57.25–27.90	52.60–27.30	50.50–26.80	50.20–28.05	54.90–26.75	50.15–27.20	49.35–26.80	44.50–27.40

Fig. 4. Temperature distribution in PV/T collector for design A.

$$\text{Subject to} \begin{cases} d_i - w\varphi(x_i) + b_i \leq \varepsilon + \xi_i \\ w\varphi(x_i) + b_i - d_i \leq \varepsilon + \xi_i^* \\ \xi_i, \quad \xi_i^* \geq 0, \quad i = 1, \ldots, l \end{cases}$$

where $(1/2)\,||w||^2$ is the regularization term, C is the error penalty factor used to regulate the difference between the regularization term and empirical error, ε is the loss function which equates to approximation accuracy of the training data point and l is the number of elements in the training data set.

Eq. (9) can be solved using the Lagrange multiplier and optimality constraints, hence obtained a generic function given as

$$f\left(x, a_i a_i^*\right) = \sum_{i=1}^{n} (a_i - a_i^*) K(x, x_i) + b \tag{12}$$

where $K(x, x_i) = \varphi(x_i)\varphi(x_j)$ and the term $K(x_i, x_j)$ is called the kernel function, which is product of the two inner vector x_i and x_j in the feature space $\varphi(x_i)$ and $\varphi(x_j)$ respectively.

There are four basic kernel functions provided by SVM, namely linear, sigmoid, polynomial and radial basis function. Radial basis function (RBF) has been proved to be the best kernel function due to its computational efficiency, simplicity, reliability, ease of adapting to optimization and other adaptive techniques as well as its

adaptability in handling parameters that are more complex [61,62]. The non-linear radial basis kernel function is defined as:

$$K(x_i, x_j) = \exp\left(-\gamma||x_i - x_j||^2\right) \tag{13}$$

where variable x_i and x_j are vectors in the input space, i.e. vectors of features computed from training or testing data set, γ is the regularization parameter that determines the trade-off between the fitting error minimization and the smoothness of the estimated function.

The accuracy of predictions using RBF kernel function depends on the selection of its three parameters (γ, ε and C). In this study, the optimal values of these parameters are found by the use of firefly optimization algorithm.

2.5.2. Support vector machine firefly optimization algorithm

The firefly algorithm (FFA) [41] is based on the certain behavioral pattern, i.e. the flashing characteristic of fireflies. A firefly is a kind of insects that uses the principle of bioluminescence to attract mates or prey. The luminance produced by a firefly enables others fireflies to trail its path in search of their prey. This concept of luminance production helps to develop algorithms to solve optimization problems.

The major issues in FFA development are the formulation of the objective function and the variation of the light intensity. For example, in the optimal design problem involving maximization
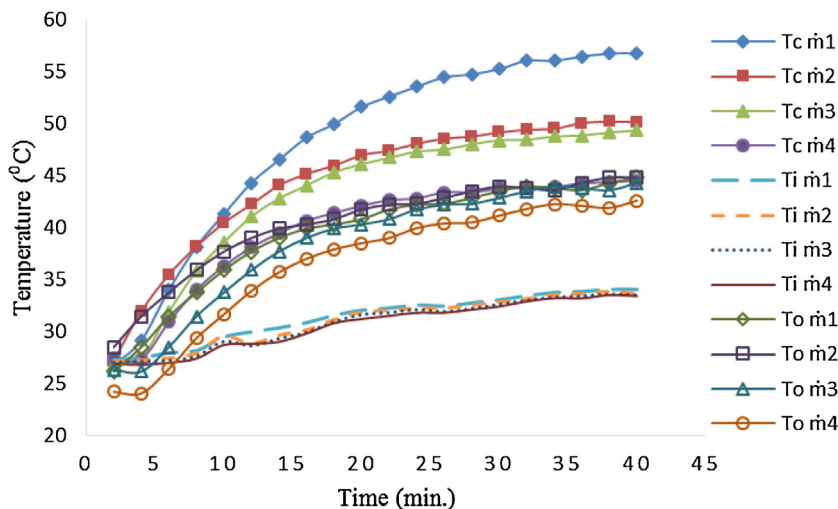

Fig. 5. Temperature distribution in PV/T collector for design B.

of objective function, the fitness function is proportional to the brightness or the amount of light emitted by the firefly. Therefore, decrease in the light intensity due to distance between the fireflies will lead to variations of intensity and thereby lessen the attractiveness among them. The light intensity with varying distance can be represented as

$$I(r) = I_o \exp\left(-\gamma r^2\right) \tag{14}$$

where I is the light intensity at distance r from a firefly, I_o represents initial light intensity, i.e. when $r = 0$ and γ is the light absorption coefficient. As a firefly's attractiveness is proportional to the light intensity observed by adjacent fireflies, the attractiveness β at a distance r from the firefly can be represented as

$$\beta(r) = \beta_o \exp\left(-\gamma r^2\right) \tag{15}$$

where β_o represents the attractiveness at distance $r = 0$.

The Cartesian distance between any two fireflies i and j is given by

$$r_{ij} = ||x_i + x_j|| = \sqrt{\sum_{k=1}^{d}\left(x_{i,k} - x_{j,k}\right)} \tag{16}$$

The movement of firefly i as attracted to another brighter firefly j can be represented as

$$\Delta x_i = \beta_o e^{-\gamma r^2}\left(x_j - x_i\right) + \alpha\varepsilon_i \tag{17}$$

where the first term in the equation is due to the attraction, the second term represents the randomization with α as randomization coefficient and ε_i is the random number vector derived from a Gaussian distribution. The next movement of firefly i is updated as

$$x_i^{i+1} = x_i + \Delta x_i \tag{18}$$

The basic steps in FFA development can be illustrated by the algorithm given in Fig. 6.

2.5.3. Discrete wavelet transform

The wavelet transform (WT) is a signal-processing algorithm developed from the Fourier transform. It represents a mathematical expression for decomposing a time series' frequency signal into different components. One of its advantages over the Fourier transform is the perfect analysis of the resulting decomposed components with well-scaled resolution, which helps in improving the capacity of the study model because it captures the needed information at different levels [63]. It is suitable for analysing data in the frequency and time domains due to its capability of extracting data from non-periodic and transient signals; hence it is very useful in time-frequency localization.

Continuous wavelet transform (CWT) of a signal $f(t)$ is a time-scale technique of signal processing that can be defined as the integral of all signals over the entire period multiplied by the scaled, shifted versions of the wavelet function $\psi(t)$, given mathematically as:

$$W_x\left(a, b, \psi\right) = \frac{1}{\sqrt{a}}\int_{-\infty}^{\infty} f(t)\,\psi^*\left(\frac{t-b}{a}\right)\,dt \tag{19}$$

where $\psi_{(t)}$ is the mother wavelet function, a is the scale index parameter (i.e., inverse of the frequency), and b is the time shifting parameter, also known as translation. The discrete wavelet transform (DWT) can be derived by discretizing Eq. (19), where the parameters a and b is given as follows:
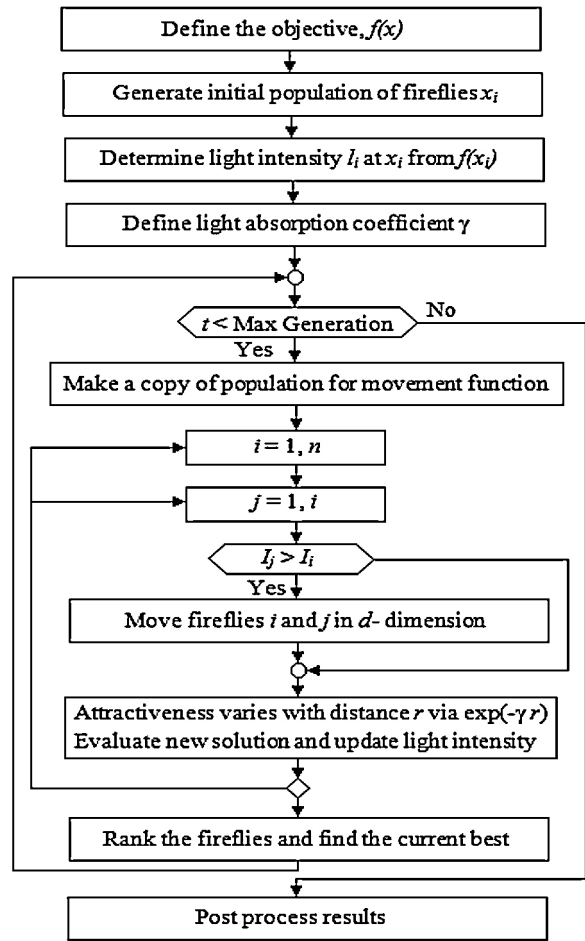
$$a = a_0^m, \quad b = na_0^m b_0$$

Fig. 6. Flow chart of Firefly Algorithm.

The variables n and m are integers. Replacing a and b in Eq. (19) gives:

$$W_x\left(m, n, \psi\right) = a_0^{-m/2}\int_{-\infty}^{\infty} f(t)\,\psi^*\left(a_0^{-m}t - nb_0\right)\,dt \tag{20}$$

In this study, wavelet analysis was used to decompose the time series of precipitation data into various components, after which the decomposed components were used as inputs for the SVM model.

2.6. Evaluating accuracy of proposed models

Predictive performances of proposed models were presented as root means square error (RMSE), coefficient of determination (R^2) and Pearson coefficient (r). These statistics are defined as follows:

(1) root-mean-square error (RMSE)

$$\text{RMSE} = \sqrt{\frac{\sum_{i=1}^{n}(P_i - O_i)^2}{n}}, \tag{21}$$

(2) Pearson correlation coefficient (r)

$$r = \frac{n\left(\sum_{i=1}^{n} O_i \cdot P_i\right) - \left(\sum_{i=1}^{n} O_i\right) \cdot \left(\sum_{i=1}^{n} P_i\right)}{\sqrt{\left(n\sum_{i=1}^{n} O_i^2 - \left(\sum_{i=1}^{n} O_i\right)^2\right) \cdot \left(n\sum_{i=1}^{n} P_i^2 - \left(\sum_{i=1}^{n} P_i\right)^2\right)}} \tag{22}$$

Table 3
User-defined parameters for SVM models.

SVM models	Parameters
SVM-Wavelet	$C = 1.45$; $\gamma = 0.342$, $\varepsilon = 0.34$
SVM-RBF	$C = 2.47$, $\gamma = 0.67$, $\varepsilon = 0.62$
SVM-FFA	$C = 1.74$, $\gamma = 0.47$, $\varepsilon = 0.27$

(3) coefficient of determination (R^2)

$$R^2 = \frac{\left[\sum_{i=1}^{n}\left(O_i - \overline{O_i}\right)\cdot\left(P_i - \overline{P_i}\right)\right]^2}{\sum_{i=1}^{n}\left(O_i - \overline{O_i}\right)\cdot\sum_{i=1}^{n}\left(P_i - \overline{P_i}\right)} \qquad (23)$$

where n is the total number of test data, P_i and O_i are known as the experimental and forecast values of electrical and thermal efficiency in PV/T system analysis, respectively.

3. Results and discussion

3.1. Performance evaluation of proposed SVM models

RBF was applied as the kernel function for the prediction of surface roughness in this study. The three parameters associated with RBF kernels are C, γ and ε. SVM model accuracy is dependent on the model parameter selection. Table 3 provides the optimal values of user-defined parameters for the proposed SVM models.

The proposed SVM-Wavelet model was obtained by combining two methods, i.e., the SVM and the Wavelet transform. The RBF was selected as the kernel function for the SVM, while the FFA was used to obtain the SVM parameters. To evaluate SVM model performance, measured surface roughness were plotted against the predicted ones. Figs. 7(a) and 8(a) presents the accuracy of developed SVM-Wavelet electrical efficiency for design A and B while Figs. 9(a) and 10(a) presents the accuracy of developed SVM-Wavelet thermal efficiency for design A and B from PV/T predictive model analysis. Similarly Figs. 7(b)–8(b) and Figs. 9(b)–10(b), Figs. 7(c)–8(c) and Figs. 9(c)–10(c) present the accuracy of developed SVM-RBF and SVM-FFA electrical and thermal efficiency of design A, B for PV/T predictive models, respectively. In every case at plotted graph it is shown basically the overall thermal efficiency for each design, theoretically which can be calculated by using Eq. (8). It can be seen that most of the points fall along the diagonal line for the SVM-Wavelet prediction model. Also, it is clear that prediction results are in very good agreement with the measured values for SVM-Wavelet model. This observation can be confirmed with high value for coefficient of determination. The number of either overestimated or underestimated values produced is limited. It is obvious that the predicted values enjoy high level precision. Here accurate prediction model of the method of SVM is studied. However, the results show that good predictions can be obtained from the SVM-Wavelet model.

It significantly improved the thermal and electrical efficiencies by the addition of fins in the collector by means of different mass flow rate. The useful heat gain varies with the mass flow rate and at a higher air velocity in channel gives the maximum heat gain. Heat is transferred to flowing air at a higher rate since the fins makes the heat transfer area increased. Again, TFMS increase the convection effect and insulator material stacks the heat in the collector.

Finally, a better thermal as well as an electrical performance approximation is possible in PV/T design using SVM prediction with high accuracy. It concludes that such integration with simplicity in design will be very effective for designers in future PV/T collector design development. This ensures the electric power supply from PV and space heating from thermal collector reduces the installation cost for various domestic applications.
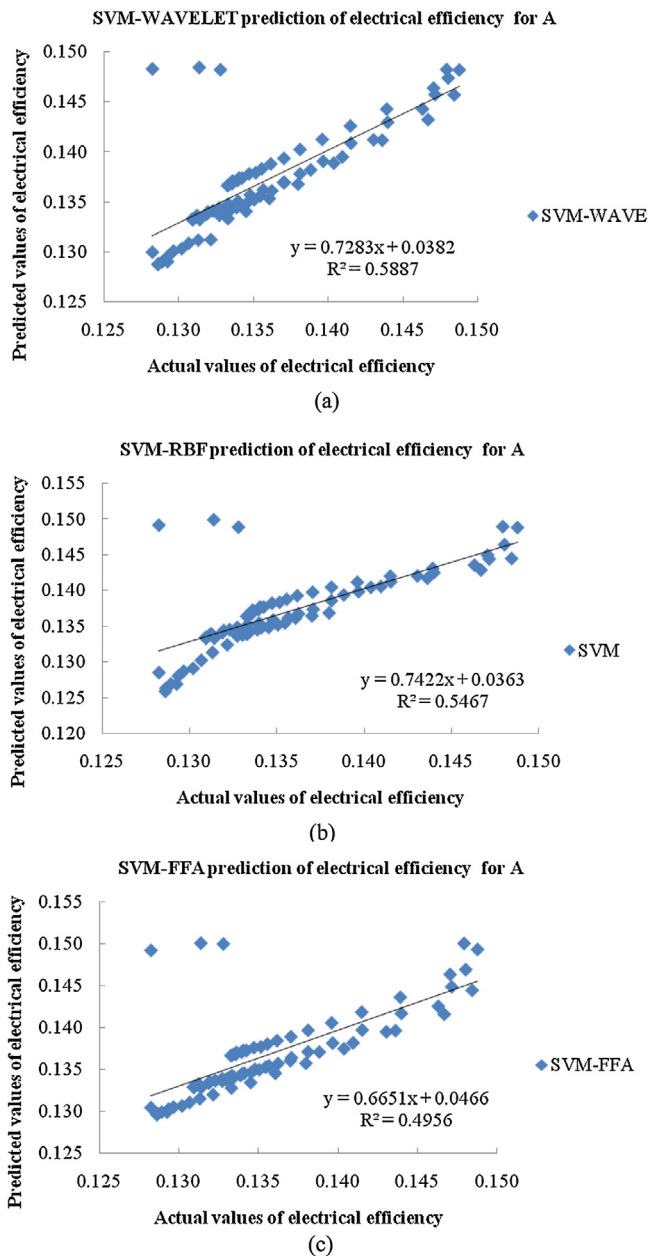

Fig. 7. Scatter plots of actual and predicted values of PV electrical efficiency using (a) SVM-Wavelet (b) SVM-RBF and (c) SVM-FFA method.

3.2. Performance comparison of SVM models

In order to demonstrate the merits of the proposed SVM models on a more definite and tangible basis, three SVM models' prediction accuracy were compared with each other. Conventional error statistical indicators, RMSE, r and R^2 were used for comparison. Tables 4–7 summarizes the prediction accuracy results for test data

Table 4
Comparative performance statistics of the SVM-Wavelet, SVM-RBF and SVM-FFA models for electrical efficiency (design A) prediction.

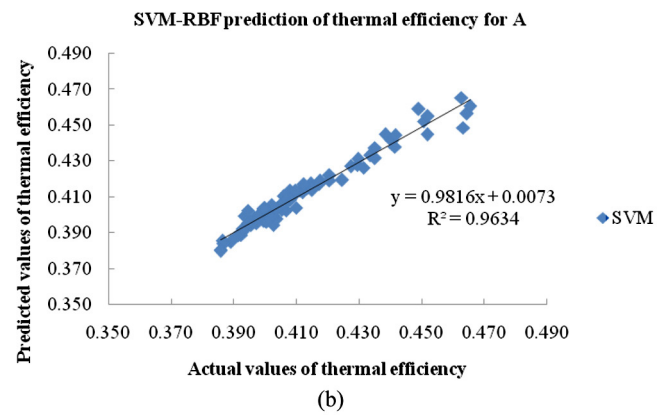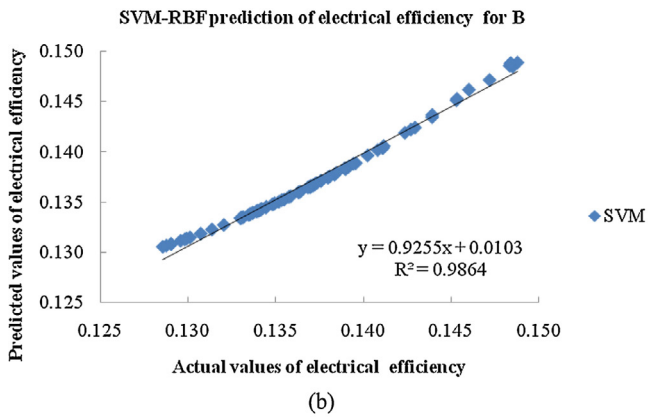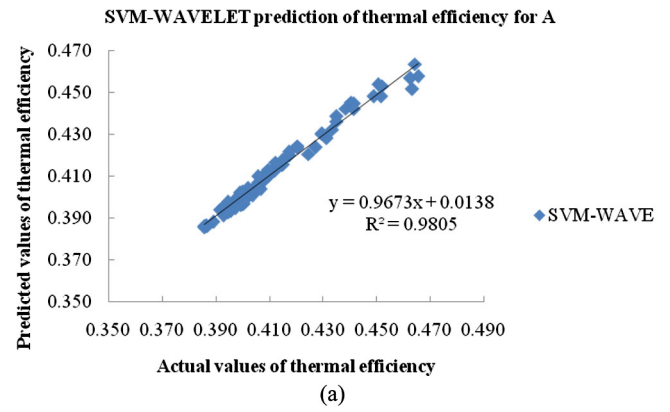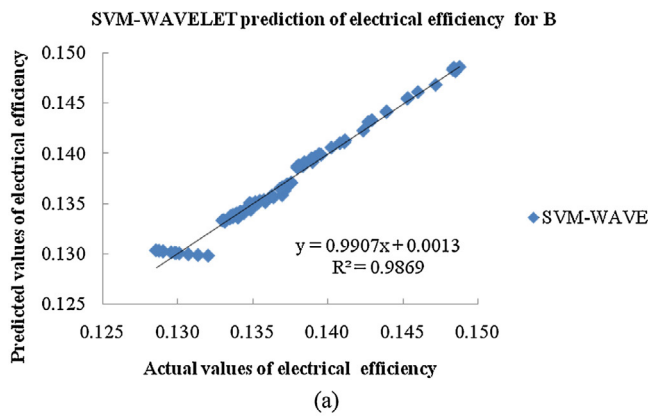| SVM model	Statistical indicator		
	RMSE	R^2	r
SVM-Wavelet	0.00385	0.5887	0.767253
SVM-RBF	0.004133	0.5467	0.739365
SVM-FFA	0.004196	0.4956	0.703994
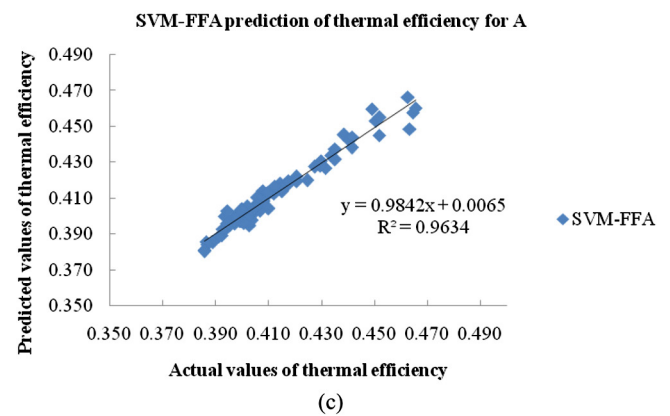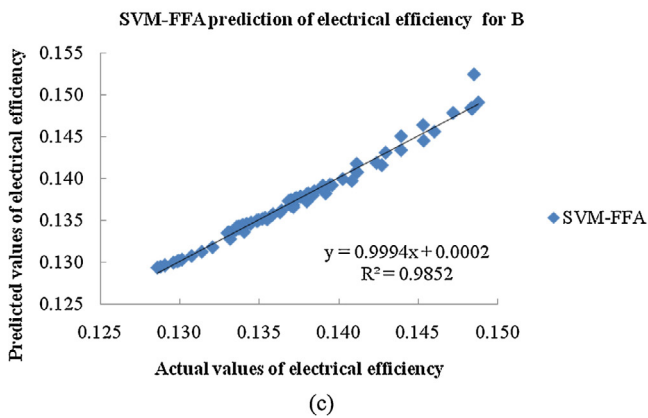
Fig. 8. Scatter plots of actual and predicted values of PV electrical efficiency using (a) SVM-Wavelet (b) SVM-RBF and (c) SVM-FFA method.

Fig. 9. Scatter plots of actual and predicted values of overall thermal efficiency using (a) SVM-Wavelet (b) SVM-RBF and (c) SVM-FFA method.

sets since training error is not a credible indicator for prediction potential of particular model.

3.3. Sensitivity analysis

In this part, to determine which input has the most impact and influence on thermal efficiencies prediction of PV/T system, a proper search was conducted from the given inputs in order to perform sensitivity analysis for all considered inputs. To achieve this, a model is built by the functions for each combination of inputs and the developed models using different inputs are then respectively trained. Subsequently, the achieved performance is reported. The results of training error in terms of RMSE for single input parameter as well as combination of 2 input parameters

Table 5
Comparative performance statistics of the SVM-Wavelet, SVM-RBF and SVM-FFA models for electrical efficiency (design B) prediction.

SVM model	Statistical indicator		
	RMSE	R^2	r
SVM-Wavelet	0.000586	0.9869	0.993431
SVM-RBF	0.000677	0.9864	0.993189
SVM-FFA	0.000644	0.9852	0.992561

Table 6
Comparative performance statistics of the SVM-Wavelet, SVM-RBF and SVM-FFA models for overall thermal efficiency (design A) prediction.

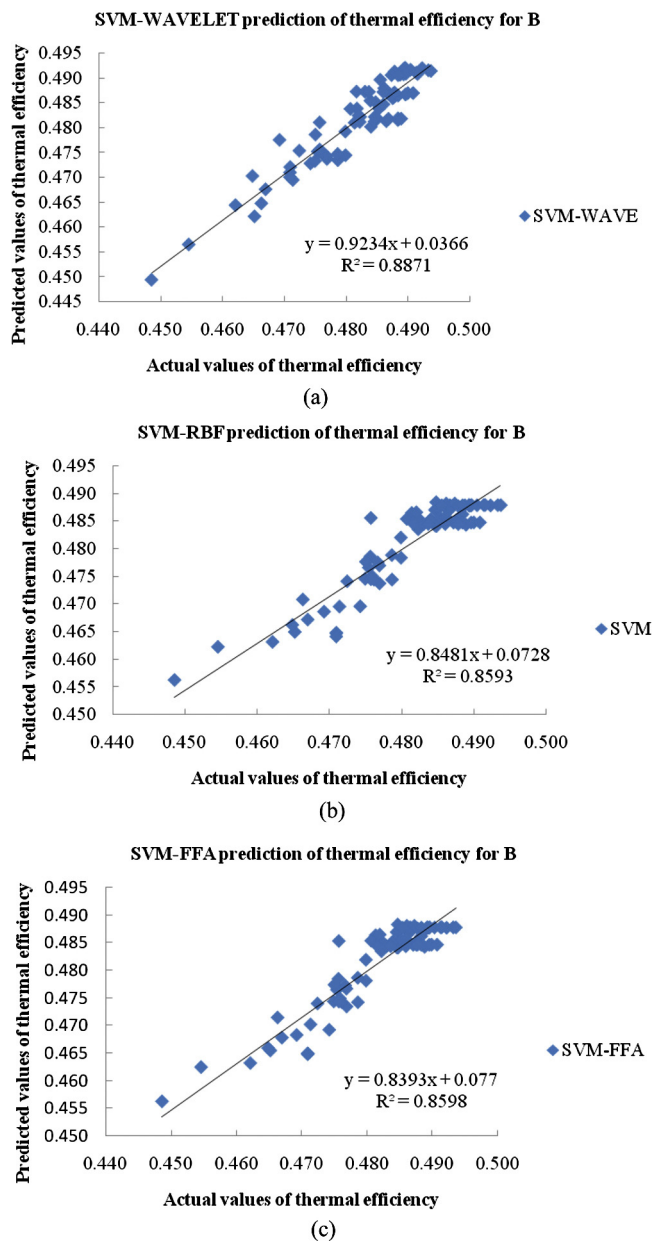| SVM model	Statistical indicator		
	RMSE	R^2	r
SVM-Wavelet	0.002872	0.9805	0.990181
SVM-RBF	0.003919	0.9634	0.981553
SVM-FFA	0.003913	0.9634	0.981537

Fig. 10. Scatter plots of actual and predicted values of overall thermal efficiency using (a) SVM-Wavelet, (b) SVM-RBF and (c) SVM-FFA method.

used to predict thermal efficiencies of PV/T system are presented in Tables 8–9, respectively. The input or set of inputs with the lowest RMSE have the most influence on the thermal efficiencies of PV/T system. According to Table 8, as expected, mass flow rate is the most influential single input parameter for prediction of thermal

Table 7
Comparative performance statistics of the SVM-Wavelet, SVM-RBF and SVM-FFA models overall thermal efficiency (design B) prediction.

SVM model	Statistical indicator		
	RMSE	R^2	r
SVM-Wavelet	0.003013	0.8871	0.941886
SVM-RBF	0.003344	0.8593	0.926965
SVM-FFA	0.003339	0.8598	0.927265

SVM-Wavelet model outperform SVM-RBF and SVM-FFA models according to the results in Tables 4–7. The predictions from the SVM models correlate highly to the actual data ($r > 0.91$).

Table 8
Sensitivity regression errors (RMSE) for one input for thermal efficiency prediction.

Input variable	RMSE
Mass flow rate (kg/s)	trn = 0.0217, chk = 0.0182
Inlet temperature (Degree Celsius)	trn = 0.0057, chk = 0.0053
Outlet temperature (Degree Celsius)	trn = 0.0041, chk = 0.0038

trn: training, chk: checking.

Table 9
Sensitivity regression errors for thermal efficiency prediction for two input parameters.

Input variable	RMSE
Mass flow rate (kg/s), inlet temperature (Degree Celsius)	trn = 0.0047, chk = 0.0044
Mass flow rate (kg/s), outlet temperature (Degree Celsius)	trn = 0.0025, chk = 0.0028
Inlet temperature (Degree Celsius), outlet temperature (Degree Celsius)	trn = 0.0032, chk = 0.0030

trn: training, chk: checking.

Table 10
Sensitivity regression errors (RMSE) for two inputs for electrical efficiency prediction.

Input variable	RMSE
c (kg/s)	trn = 0.0097, chk = 0.0082
PV cell temperature (°C)	trn = 0.0507, chk = 0.0503

trn: training, chk: checking.

efficiencies of PV/T system. It is worthwhile to mention that the training error is relevant for the sensitivity analysis. However, the checking error is also used to track overfitting between training and checking data. In terms of combination of 2 inputs, the results presented in Table 9 show that the combination of two inputs of mass flow rate and inlet temperature is identified as the most influential set of 2 inputs. It is noticed that the RMSE reduce when the number of influential variable increases from 1 to 2. For electrical efficiency the sensitivity analysis of the two inputs are given in Table 10.

4. Conclusion

The study carried out a systematic approach creating the SVM models for the prediction of electrical and thermal efficiency for two proposed PV/T design by SVM-Wavelet, SVM-RBF and SVM-FFA.

Predicted data was compared with experimental literature data and as can be seen from the statistical data that SVM models can be used with reasonable accuracy. By performance comparison, design B shows the higher performance than design A with maximum mass flow rate.

Sensitivity regression error analysis shows the negligible deviation by training and checking data over the historical data which concludes that the SVM method of analysis is more reliable in estimating PV/T performance.

Accuracy results, measured in terms of RMSE, r, R^2 and EI indicate that SVM-Wavelet predictions are superior to the SVM-RBF and the SVM-FFA.

The appropriate sensitivity analysis concludes that proper selection of input parameters plays a remarkable role to boost the accuracy of electrical and thermal efficiency prediction by the SVM algorithms under certain specification provided for PV/T collector system.

Finally, it has the further impact in reducing the design and installation cost by optimizing efficiencies of the PV/T system.

Acknowledgements

References

[1] F. Sarhaddi, et al., Exergetic performance assessment of a solar photovoltaic thermal (PV/T) air collector, Energy Build. 42 (11) (2010) 2184–2199.
[2] F. Hussain, et al., Design development and performance evaluation of photovoltaic/thermal (PV/T) air base solar collector, Renewable Sustainable Energy Rev. 25 (0) (2013) 431–441.
[3] M. Caner, E. Gedik, A. Keçebaş, Investigation on thermal performance calculation of two type solar air collectors using artificial neural network, Expert Syst. Appl. 38 (3) (2011) 1668–1674.
[4] P.G. Charalambous, et al., Optimization of the photovoltaic thermal (PV/T) collector absorber, Sol. Energy 85 (5) (2011) 871–880.
[5] D. Kamthania, S. Nayak, G.N. Tiwari, Performance evaluation of a hybrid photovoltaic thermal double pass facade for space heating, Energy Build. 43 (9) (2011) 2274–2281.
[6] R.S. Kamel, A.S. Fung, Modeling, simulation and feasibility analysis of residential BIPV/T + ASHP system in cold climate—Canada, Energy Build. 82 (2014) 758–770.
[7] V. Delisle, M. Kummert, A novel approach to compare building-integrated photovoltaics/thermal air collectors to side-by-side PV modules and solar thermal collectors, Sol. Energy 100 (2014) 50–65.
[8] S.-Y. Wu, et al., A heat pipe photovoltaic/thermal (PV/T) hybrid system and its performance evaluation, Energy Build. 43 (12) (2011) 3558–3567.
[9] P.G. Charalambous, et al., Photovoltaic thermal (PV/T) collectors: a review, Appl. Therm. Eng. 27 (2–3) (2007) 275–286.
[10] Y.-S. Lee, L.-I. Tong, Predicting high or low transfer efficiency of photovoltaic systems using a novel hybrid methodology combining rough set theory, data envelopment analysis and genetic programming, Energies 5 (3) (2012) 545–560.
[11] J. Tamayo Vera, T. Laukkanen, K. Sirén, Multi-objective optimization of hybrid photovoltaic–thermal collectors integrated in a DHW heating system, Energy Build. 74 (2014) 78–90.
[12] N. Aste, C. del Pero, F. Leonforte, Water flat plate PV–thermal collectors: a review, Sol. Energy 102 (0) (2014) 98–115.
[13] T.T. Chow, et al., Energy and exergy analysis of photovoltaic–thermal collector with and without glass cover, Appl. Energy 86 (3) (2009) 310–316.
[14] F. Shan, L. Cao, G. Fang, Dynamic performances modeling of a photovoltaic–thermal collector with water heating in buildings, Energy Build. 66 (2013) 485–494.
[15] S.C. Solanki, S. Dubey, A. Tiwari, Indoor simulation and testing of photovoltaic thermal (PV/T) air collectors, Appl. Energy 86 (11) (2009) 2421–2428.
[16] S. Dubey, S.C. Solanki, A. Tiwari, Energy and exergy analysis of PV/T air collectors connected in series, Energy Build. 41 (8) (2009) 863–870.
[17] K. Touafek, M. Haddadi, A. Malek, Design and modeling of a photovoltaic thermal collector for domestic air heating and electricity production, Energy Build. 59 (2013) 21–28.
[18] F. Shan, et al., Dynamic characteristics modeling of a hybrid photovoltaic–thermal solar collector with active cooling in buildings, Energy Build. 78 (2014) 215–221.
[19] H.A. Zondag, et al., The yield of different combined PV–thermal collector designs, Sol. Energy 74 (3) (2003) 253–269.
[20] J.K. Tonui, Y. Tripanagnostopoulos, Improved PV/T solar collectors with heat extraction by forced or natural air circulation, Renewable Energy 32 (4) (2007) 623–637.
[21] T.T. Chow, A review on photovoltaic/thermal hybrid solar technology, Appl. Energy 87 (2) (2010) 365–379.
[22] A. Ibrahim, et al., Recent advances in flat plate photovoltaic/thermal (PV/T) solar collectors, Renewable Sustainable Energy Rev. 15 (1) (2011) 352–365.
[23] A. Kumar, P. Baredar, U. Qureshi, Historical and recent development of photovoltaic thermal (PVT) technologies, Renewable Sustainable Energy Rev. 42 (0) (2015) 1428–1436.
[24] P. Dupeyrat, C. Ménézo, S. Fortuin, Study of the thermal and electrical performances of PVT solar hot water system, Energy Build. 68 (Part C(0)) (2014) 751–755.
[25] Y. Tripanagnostopoulos, Aspects and improvements of hybrid photovoltaic/thermal solar energy systems, Sol. Energy 81 (9) (2007) 1117–1131.
[26] R. Liang, et al., Performance evaluation of new type hybrid photovoltaic/thermal solar collector by experimental study, Appl. Therm. Eng. 75 (2015) 487–492.
[27] Y. Varol, et al., Forecasting of thermal energy storage performance of Phase Change Material in a solar collector using soft computing techniques, Expert Syst. Appl. 37 (4) (2010) 2724–2732.
[28] W.-Z. Lu, W.-J. Wang, Potential assessment of the "support vector machine" method in forecasting ambient air pollutant trends, Chemosphere 59 (5) (2005) 693–701.
[29] T. Asefa, et al., Multi-time scale stream flow predictions: the support vector machines approach, J. Hydrol. 318 (1–4) (2006) 7–16.
[30] P. Jain, J.M. Garibaldi, J.D. Hirst, Supervised machine learning algorithms for protein structure classification, Comput. Biol. Chem. 33 (3) (2009) 216–223.
[31] Y. Ji, S. Sun, Multitask multiclass support vector machines: model and experiments, Pattern Recognit. 46 (3) (2013) 914–924.
[32] J. Alonso, A. Villa, A. Bahamonde, Improved estimation of bovine weight trajectories using Support Vector Machine Classification, Comput. Electron. Agric. 110 (0) (2015) 36–41.
[33] M. Fu, Y. Tian, F. Wu, Step-wise support vector machines for classification of overlapping samples, Neurocomputing 155 (0) (2015) 159–166.
[34] F. Kaytez, et al., Forecasting electricity consumption: a comparison of regression analysis, neural networks and least squares support vector machines, Int. J. Electr. Power Energy Syst. 67 (0) (2015) 431–438.
[35] R. Zhang, W. Wang, Facilitating the applications of support vector machine by using a new kernel, Expert Syst. Appl. 38 (11) (2011) 14225–14230.
[36] J.S. Angelo, H.S. Bernardino, H.J.C. Barbosa, Ant colony approaches for multiobjective structural optimization problems with a cardinality constraint, Adv. Eng. Softw. 80 (0) (2015) 101–115.
[37] E. Assareh, et al., Application of PSO (particle swarm optimization) and GA (genetic algorithm) techniques on demand estimation of oil in Iran, Energy 35 (12) (2010) 5223–5229.
[38] M. Dorigo, G. Caro, L. Gambardella, Ant algorithms for discrete optimization, Artif. Life 5 (2) (1999) 137–172.
[39] M. Dorigo, T. Stützle, The ant colony optimization metaheuristic: Algorithms, applications, and advances, in: F. Glover, G.A. Kochenberger (Eds.), Handbook of Metaheuristics, Kluwer, 2003, pp. 251–258.
[40] X.-S. Yang, S. Deb, Cuckoo search: recent advances and applications, Neural Comput. Appl. 24 (1) (2014) 169–174.
[41] X.S. Yang, Firefly algorithms for multimodal optimization, in: O. Watanabe, T. Zeugmann (Eds.), Stochastic Algorithms: Foundations and Appplications, SAGA 2009, Lecture Notes in Computer Science, vol. 5792, Springer-Verlag, Berlin, 2009, pp. 169–178.
[42] I. Fister, X.-S. Yang, J. Brest, A comprehensive review of firefly algorithms, Swarm Evol. Comput. 13 (2013) 34–46.
[43] X.-S. Yang, Multiobjective firefly algorithm for continuous optimization, Eng. Comput. 29 (2) (2013) 175–184.
[44] S. Ch, et al., A Support Vector Machine-Firefly Algorithm based forecasting model to determine malaria transmission, Neurocomputing 129 (2014) 279–288.
[45] T. Kanimozhi, K. Latha, An integrated approach to region based image retrieval using firefly algorithm and support vector machine, Neurocomputing 151 (2015) 1099–1111.
[46] A. Sözen, T. Menlik, S. Ünvar, Determination of efficiency of flat-plate solar collectors using neural network approach, Expert Syst. Appl. 35 (4) (2008) 1533–1539.
[47] H. Esen, et al., Modeling a ground-coupled heat pump system by a support vector machine, Renewable Energy 33 (8) (2008) 1814–1823.
[48] H. Esen, et al., Modelling of a new solar air heater through least-squares support vector machines, Expert Syst. Appl. 36 (7) (2009) 10673–10682.
[49] H. Esen, et al., Artificial neural network and wavelet neural network approaches for modelling of a solar air heater, Expert Syst. Appl. 36 (8) (2009) 11240–11248.
[50] J. Adamowski, H.F. Chan, A wavelet neural network conjunction model for groundwater level forecasting, J. Hydrol. 407 (1) (2011) 28–40.
[51] A.M. Kalteh, Monthly river flow forecasting using artificial neural network and support vector regression models coupled with wavelet transform, Comput. Geosci. 54 (2013) 1–8.
[52] S. Dubey, G.N. Tiwari, Analysis of PV/T flat plate water collectors connected in series, Sol. Energy 83 (9) (2009) 1485–1498.
[53] A. Tiwari, M.S. Sodha, Performance evaluation of solar PV/T system: an experimental validation, Sol. Energy 80 (7) (2006) 751–759.
[54] A.S. Joshi, et al., Performance evaluation of a hybrid photovoltaic thermal (PV/T) (glass-to-glass) system, Int. J. Therm. Sci. 48 (1) (2009) 154–164.
[55] R. Kumar, M.A. Rosen, Performance evaluation of a double pass PV/T solar air heater with and without fins, Appl. Therm. Eng. 31 (8–9) (2011) 1402–1410.
[56] F. Ozgen, M. Esen, H. Esen, Experimental investigation of thermal performance of a double-flow solar air heater having aluminium cans, Renewable Energy 34 (11) (2009) 2391–2398.
[57] J.K. Tonui, Y. Tripanagnostopoulos, Air-cooled PV/T solar collectors with low cost performance improvements, Sol. Energy 81 (4) (2007) 498–511.
[58] M.S. Buker, B. Mempouo, S.B. Riffat, Performance evaluation and techno-economic analysis of a novel building integrated PV/T roof collector: an experimental validation, Energy Build. 76 (2014) 164–175.
[59] B.J. Huang, et al., Performance evaluation of solar photovoltaic/thermal systems, Sol. Energy 70 (5) (2001) 443–448.
[60] V.N. Vapnik, Statistical Learning Theory, Wiley Interscience, New York, NY, 1998.
[61] S. Rajasekaran, S. Gayathri, T.-L. Lee, Support vector regression methodology for storm surge predictions, Ocean Eng. 35 (16) (2008) 1578–1587.
[62] Z. Ramedani, et al., Potential of radial basis function based support vector regression for global solar radiation prediction, Renewable Sustainable Energy Rev. 39 (2014) 1005–1011.
[63] K.-P. Wu, S.-D. Wang, Choosing the kernel parameters for support vector machines by the inter-cluster distance in the feature space, Pattern Recognit. 42 (5) (2009) 710–717.